Fano resonances in the conductance of quantum dots with mixed dynamics

Michel Mendoza,[1] Peter A. Schulz,[2] Raúl O. Vallejos,[3] and Caio H. Lewenkopf[4,5]
[1]*Centro de Ciências Naturais e Humanas, Universidade Federal do ABC (UFABC), 09210-170 Santo André, Brazil*
[2]*Instituto de Física Gleb Wataghin, UNICAMP, Caixa Postal 6165, 13083-970 Campinas, Brazil*
[3]*Centro Brasileiro de Pesquisas Físicas, R. Dr. Xavier Sigaud 150, 22290-180 Rio de Janeiro, Brazil*
[4]*Departamento de Física Teórica, Universidade do Estado do Rio de Janeiro, 20550-900 Rio de Janeiro, Brazil*
[5]*Department of Physics, Harvard University, Cambridge, Massachusetts 02138, USA*
(Received 26 November 2007; published 8 April 2008)

We study the conductance fluctuations of an open quantum dot with underlying mixed dynamics. In addition to smooth conductance fluctuations, typical of chaotic quantum dots, we observe the occurrence of many sharp conductance peaks. Those are associated with localized states in the quantum dot and display a variety of Fano shape resonances. We show that the Fano q parameter in the presence of time-reversal symmetry is, in general, complex. We discuss the origin of the different Fano parameters and present a numerical study to support our theory.

DOI: 10.1103/PhysRevB.77.155307 PACS number(s): 73.23.Ad, 05.45.Mt, 72.20.Dp, 03.65.Sq

I. INTRODUCTION

Quantum interference is at the heart of the physics of mesoscopic phenomena and is beautifully manifested by universal conductance fluctuations (UCFs) and weak localization.[1] At sufficiently low temperatures, both the UCF and the weak localization peak have been experimentally observed in open chaotic quantum dots (QDs) containing $N \gtrsim 100$ electrons. Theory addresses these results by means of the Landauer formula that relates the linear conductance in quantum coherent systems to the transmission probability. While the universal aspects of experiments, such as conductance distributions and conductance autocorrelation functions, have been successfully described by the random matrix theory (for recent reviews, see Refs. 2 and 3), system specific properties, such as magnetic correlation lengths, were accurately addressed by the chaotic semiclassical scattering theory.[4] The latter also explicitly shows how universal fluctuations arise from the interference of all possible transmission pathways.[4]

Quantum interference, however, can be built from just two interfering paths, giving rise to a variety of resonance shapes, as explained in a seminal paper by Fano.[5] Albeit observed in numerous systems, including neutron scattering,[6] atomic photoionization,[7] Raman scattering,[8] optical absorption in quantum wells,[9] scanning tunneling microscopy,[10] and microwave scattering,[11] Fano resonances have received less attention in mesoscopic phenomena.

Experimentally, Fano resonances have been observed first in QDs at the Kondo regime.[12] More recently, by embedding a Coulomb blockaded quantum dot in an Aharonov–Bohm ring interferometer, a variety of Fano conductance shapes were measured.[13] Conductance measurements exploring different geometries, such as a quantum wire with a side-coupled quantum dot,[14] a one-lead quantum dot,[15] and a ring with side-coupled dot,[16] provide more insight into the Fano problem in mesoscopic systems. It is noteworthy that in all of these experiments, the quantum dots were taken either at the Coulomb blockade regime or at the Kondo regime, where electronic interactions are very important.

The occurrence of conductance dips in ballistic Aharonov–Bohm rings was theoretically investigated almost 20 years ago.[17] Further, early theoretical works examined the possibility of Fano shapes in the transmission through one-dimensional waveguides[18,19] and waveguides with resonantly coupled cavities.[20] More recently, Fano resonances have also been found in numerical investigations on the influence of a smooth confining potential (leading to mixed dynamics) on open quantum dots.[21,22] These findings triggered proposals for interesting applications, such as controlling Fano line shapes[23] and using them for the readout of single spins.[24]

Given this wealth of theoretical work, why is the experimental observation of Fano line-shape resonances so elusive in open quantum dots? This is the main question we try to answer in this study. We find that the occurrence of conductance Fano shapes is favored in QDs when their classical dynamics is mixed. In this regime, the transmission is characterized by (i) narrow resonances corresponding to localized states, trapped either on tori of stable motion or cantori, (ii) fluctuations typical to chaotic motion, and (iii) fast (nonresonance) scattering processes, depending on the QD geometry. The interference between these scattering processes gives rise to a variety of Fano conductance shapes. We show that the resonance line shapes can be cast by an expression similar to the standard Fano formula,[5] but with a complex q. This result is quite general for multichannel scattering and is applicable whenever a system has a narrow resonance whose lifetime is much longer than all of the other relevant scattering time scales.

The paper is organized as follows. In Sec. II, we present the cosine billiard, the model we employ to investigate the conductance in quantum dots with mixed dynamics. The numerical method used to solve the scattering problem is presented in Sec. III. The general Fano theory for multiple continua and multiple resonances is reviewed in Sec. IV. The numerical analysis of the conductance and Fano resonances in the cosine billiard is presented in Sec. V. In our conclusion, we discuss our findings in view of the current experiments.

II. MODEL SYSTEM

We use an open billiard to model the electron single-particle properties of lateral open quantum dots. Hard-wall confinement potentials are expected to accurately model dots whose typical size L is much larger than the Fermi wavelength λ_F.[25] This condition is met by quantum dots containing at least 10^2-10^3 electrons, which is quite typical in experiments.[26]

We chose the cosine billiard[27] to guide our analysis. This is a convenient model because (a) the cosine billiard shape parameters can be tuned so that the classical dynamics goes from the chaotic to the mixed regime; (b) its classical dynamics is well understood; and (c) the quantum numerical analysis is quite amenable.[28,29]

The cosine billiard is defined as follows: let the electrons move in the (x,y) plane. The open cosine billiard is defined by two disjoint boundaries on which the electrons scatter elastically. One boundary is given by $y_1=0$. The other is

$$y_2(x) = W + \frac{M}{2}\left[1 + \cos\left(\frac{2\pi x}{L}\right)\right], \tag{1}$$

for $-L/2 \leqslant x \leqslant L/2$ and $y_2(x)=W$ for $|x|>L/2$.

We identify an "inner" region $|x|<L/2$ with the quantum dot and an "outer" region $|x|>L/2$ with leads connected to reservoirs in thermal equilibrium. In the leads, the electron energy E can be decomposed as the sum of $E_\perp$ and $E_\parallel$, the latter corresponding to the free longitudinal motion. We consider scattering processes where electrons come from the left $x\to-\infty$ with a certain transversal energy $E_\perp$, enter the quantum dot, and emerge at its left $(x<-L/2)$ or right contact $(x>L/2)$ with an energy $E'_\perp$.

The main features of the cosine billiard single-particle classical dynamics can be understood by simple considerations: the vertical trajectory at $x=0$ is stable if the radius of curvature of the cosine boundary at $x=0$ is larger than the billiard width at $x=0$. This amounts to requiring $L^2/2\pi^2 M > W+M$. In this case, the vertical trajectory is surrounded by a stability island that can be clearly seen, e.g., in a Poincaré section at $y=0^+$. The island is composed mainly of trajectories that display a quasiperiodic motion and remain close to $x=0$. In the mixed dynamics regime, as usual, the central island is surrounded by other smaller islands, regions of chaotic dynamics, KAM tori, etc. When the billiard is open and coupled to leads (or waveguides), the island does not explicitly participate in the scattering process because it is not accessible from outside.

The classical transport properties of the cosine billiard as a function of the parameters W/L and M/L are well understood.[27] From the wide range of parameter values where the system shows mixed dynamics, we chose to work with $W/L=0.18$ and $M/L=0.10$, for which both the classical and quantum cases have been extensively studied. The inset in Fig. 1 illustrates the cosine billiard geometry used in this study.

When quantum scattering is considered, the stability island centered at $x=0$ manifests itself through localized quasibound states weakly coupled to the continuum. These states correspond to complex poles of the S matrix that can lie very close to the real axis, i.e., have a decay width much smaller than average resonance spacing. Localized states rarely overlap with each other and appear as isolated resonances in the scattering observables, i.e., cross sections, conductance, or density of states. The remaining resonances correspond to delocalized states and are expected to have large decay widths and overlap. We shall quantitatively address these issues in the forthcoming sections.

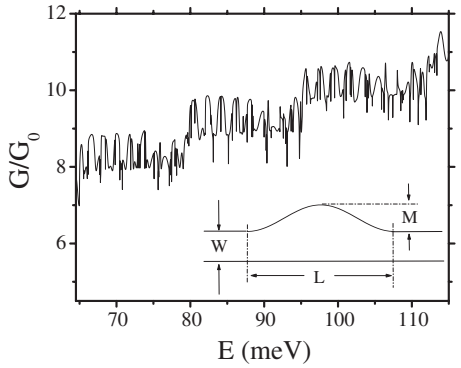

FIG. 1. Conductance in units of $G_0=2e^2/h$ versus energy in meV for the cosine billiard shaped quantum dot with $M/L\approx0.10$ and $W/L\approx0.18$. The conductance plateaus correspond to $N=9$ up to $N=11$. Inset: Cosine billiard geometry.

III. LANDAUER CONDUCTANCE OF THE COSINE BILLIARD

In this section, we describe how we compute the S matrix of our model system and present a qualitative discussion of the transmission fluctuations.

The asymptotic modes of the scattering problem are defined as standard: due to the perpendicular confinement, the energy $E_\perp$ is quantized, namely, $(E_\perp)_n=\hbar^2/2m^*(\pi n/W)^2$, where m^* is the electron effective mass and n is an integer number that labels the propagating modes at the left and right sides of the quantum dot. The transversal wave functions are $\chi_n(y)=\sqrt{2/W}\sin(\pi n y/W)$. The number of open modes per lead is N, the largest integer such that $(E_\perp)_N \leqslant E$.

The probability amplitude for an electron to be scattered from a channel n to a channel m is given by the scattering matrix element S_{mn}. For convenience, we write the S matrix as[30]

$$S = \begin{pmatrix} r & t' \\ t & r' \end{pmatrix}, \tag{2}$$

where r (r') is the reflection matrix for the channels at the left (right) and t (t') is the transmission matrix from left (right) to right (left) channels.

The Landauer formula[1] relates the linear conductance to the transmission probability. We consider the zero temperature limit to write

$$G = \frac{2e^2}{h}\mathrm{tr}(t^\dagger t), \tag{3}$$

where the factor 2 accounts for the spin degeneracy. We present our results in terms of the dimensionless conductance

G/G_0, where $G_0=2e^2/h$, which is equivalent to transmission $T\equiv \mathrm{tr}(t^\dagger t)$.

We compute the S-matrix elements by using the Fisher–Lee formula,[31] namely,

$$S_{nm}(E) = -\delta_{nm} + i\hbar\sqrt{v_n v_m}\int_0^W dy_q \int_0^W dy_p \chi_n(y_q) G^r_{qp} \times (y_q, y_p; E)\chi_m(y_p), \tag{4}$$

where $\chi_m(y_p)$ is the transversal wave function of an electron in the mode m at lead p, and v_m is its velocity. $G^r_{qp}(y_q,y_p;E)$ is a shorthand for the open cavity retarded Green's function $G^r(\mathbf{r}_q,\mathbf{r}_p;E)$, where $\mathbf{r}_p=(x_p,y_p)$ and $x_p=\pm L/2$, which depends on whether p denotes the left or right lead. (See, for instance, Ref. 32 for more details).

We compute $G^r_{qp}(y_q,y_p;E)$ on a discrete lattice by using the recursive Green's function method.[32–34] The same method is also used to obtain the local density of states (LDOS), $\rho(\mathbf{r})=-(1/\pi)\mathrm{Im}\, G^r(\mathbf{r},\mathbf{r};E)$.

To avoid finite mesh size effects in our numerical analysis (Sec. V), we considered $\lambda/a>8$, where a is the lattice parameter, and $\lambda=\lambda(E)$ is the electron wavelength at energy E. For the energy range addressed in this study, we take $M_s=22$ and $W_s=40$ transversal sites and $L_s=221$ longitudinal ones. To model realistic device dimensions,[26] we take $a=20$ Å. The cosine billiard parameters become $M=0.044$ μm, $W=0.080$ μm, and $L=0.442$ μm. The electron effective mass at the bottom of the GaAs conduction band, $m^*=0.067m_0$, leads to nearest neighbor tight-binding hopping parameters $V_{x,y}=-\hbar^2/2m^*a^2=-0.142$ eV.

Figure 1 shows the dimensionless conductance G/G_0 as a function of the energy E. As the energy is varied, one observes jumps in the average conductance. Those jumps appear at the threshold energies for channel openings in the leads. More interesting is the observation that at every conductance plateau, corresponding to a fixed number of channels N, the transmission displays both slow energy fluctuations (on energy scales $\Gamma_{\mathrm{cor}}\sim 1$ meV) and narrow resonances (of widths $\Gamma<0.1$ meV). The latter occur in a variety of shapes. The theory underpinning such shapes is addressed in what follows.

Before we proceed, there is an important point to address. We neglect electron-electron interactions as widely justified for open quantum dots, where the electron dwell time in the dot τ_D is typically much shorter than the charging time τ_C.[2] However, the resonances corresponding to localized states are narrow and can easily have lifetimes that exceed τ_C, a situation analogous to the Coulomb blockade regime. This makes the situation we analyze quite unique: There are no constraints for electrons to flow through the QD, but the transport via the stability islands requires a certain energy to overcome charging effects. Despite this, with certain care (taken in this paper), the single-particle description can still be used, namely, (a) by treating every narrow resonance separately and restricting the analysis to small energy windows around each of them (far from the adjacent narrow resonances that can contribute with cotunneling), and by (b) assuming that the screening is short ranged (as standard in semiconductor quantum dots[2]) and, hence, the electron dynamics is barely modified by excess charges.

IV. FANO LINE SHAPES IN THE PRESENCE OF MANY RESONANCES AND MANY CONTINUA

In this section, we discuss how multichannel resonance scattering in a system with mixed dynamics gives rise to Fano resonances in the transmission.

Let us begin by considering the case of a single resonance with a complex pole $\varepsilon_0=E_0-i\Gamma_0/2$ and a single lead with $N=1$. Although the single-lead case has little direct relevance for the conductance, it provides insight into the origin of the Fano resonance profiles. In the presence of a single channel, the S matrix is just a complex number with unit modulus, parametrized as $S=e^{2i\phi}(E-\varepsilon_0^*)/(E-\varepsilon_0)$. Then the cross section, $\sigma=4\pi\lambda^2(1-\mathrm{Re}\, S)$,[35] becomes

$$\sigma \propto \frac{(q+\epsilon)^2}{\epsilon^2+1}, \tag{5}$$

where $\epsilon=2(E-E_0)/\Gamma_0$ and $q=-\cot\phi$. This is essentially Fano's famous result,[5] here obtained by using the S matrix pole parametrization.

The transmission analysis for the multichannel case follows the same lines. Let us write the open quantum dot retarded Green's function, appearing in Eq. (4), in the spectral representation, namely,[32]

$$G^r(\mathbf{r},\mathbf{r}';E) = \sum_\mu \frac{\psi_\mu(\mathbf{r})\varphi_\mu^*(\mathbf{r}')}{E-E_\mu+i\Gamma_\mu/2}, \tag{6}$$

where ψ_μ and φ_μ are the right and left eigenfunctions of the effective Hamiltonian of the open cavity, corresponding to the complex energy $\varepsilon_\mu=E_\mu-i\Gamma_\mu/2$. Defining

$$\gamma_{n\mu} = \sqrt{\hbar v_n}\int_0^W dy_p \chi_n(y_p)\psi_\mu(x_p,y_p),$$

$$\tilde{\gamma}_{m\mu} = \sqrt{\hbar v_m}\int_0^W dy_p \chi_m(y_p)\varphi_\mu(x_p,y_p), \tag{7}$$

we arrive at

$$t_{nm}(E) = i\sum_\mu \frac{\gamma_{n\mu}\tilde{\gamma}^*_{m\mu}}{E-E_\mu+i\Gamma_\mu/2}. \tag{8}$$

Let us now focus our attention on the energy interval around a single narrow resonance with a pole at $\varepsilon_\nu=E_\nu-i\Gamma_\nu/2$. The transmission matrix elements read

$$t_{nm}(E) = t^{\mathrm{bg}}_{nm}(E) + i\frac{\gamma_{n\nu}\tilde{\gamma}^*_{m\nu}}{E-E_\nu+i\Gamma_\nu/2}. \tag{9}$$

The background transmission matrix element $t^{\mathrm{bg}}_{nm}(E)$ accounts for the contribution of all but the νth resonance, namely,

$$t^{\mathrm{bg}}_{nm}(E) = i\sum_{\mu\neq\nu} \frac{\gamma_{n\mu}\tilde{\gamma}^*_{m\mu}}{E-E_\mu+i\Gamma_\mu/2}. \tag{10}$$

In this parametrization, prompt processes correspond to a few poles ε_μ with a decay width $\Gamma_\mu \gg \Gamma_{\mathrm{cor}}$, as nicely dis-

cussed in Ref. 36. Hence, we write the partial transmission coefficients as

$$|t_{nm}(E)|^2 = |t_{nm}^{\mathrm{bg}}(E)|^2 \frac{|q' + \epsilon|^2}{\epsilon^2 + 1}, \tag{11}$$

with $\epsilon = 2(E - E_\nu)/\Gamma_\nu$, as in the standard Fano definition. In contrast, the shape parameter q' is, in general, complex and given by

$$q' = i - \frac{2i}{t_{nm}^{\mathrm{bg}}} \frac{\gamma_{n\nu} \tilde{\gamma}_{m\nu}^*}{\Gamma_\nu}. \tag{12}$$

In the vicinity of the resonance peak, $E = E_\nu$, t_{nm}^{bg} can be taken as energy independent. More specifically, for an energy window of the order of the resonance width, this approximation requires $\Gamma_\nu \ll \Gamma_{\mathrm{cor}}$. As we already discussed, this inequality is typical in the transmission spectrum of mixed systems. In contrast, writing $|t_{nm}(E)|^2$ as Eq. (11) becomes extremely arbitrary in the absence of a clear separation of energy scales, a situation met in chaotic quantum dots.

The conductance, which is a sum of partial transmission coefficients, also displays a Fano profile for an isolated resonance. Its shape parameter q is a combination of the q's of all transmission coefficients.[37]

The derivation of a complex q' we present is tailor-made for the Fisher–Lee S matrix. However, the result we obtain is quite general to multichannel resonance scattering, since Eq. (9) can be written just by invoking the symmetries and the analytic properties of the S matrix, as shown in the Appendix.

We remark that a complex line-shape parameter q has been proposed to fit Fano resonances experimentally observed in the conductance of a quantum dot embedded in an Aharonov–Bohm ring.[13] This procedure was first justified, in a similar way as here, by considering that one arm of the interferometer provides a featureless background.[37] Complex q's also appear in a single-channel scattering, e.g., when two thin resonances overlap.[38]

Another recent noteworthy development gives a geometric interpretation of the shape parameter q (Refs. 39 and 40) by expressing the scattering problem of a single resonance and $N=1$ in terms of conical intersections. However, the extension of this idea to the multichannel case does not appear to be straightforward.

V. NUMERICAL ANALYSIS

We are now ready to quantitatively address the main transmission features of the cosine billiard.

Let us begin with the average conductance. Due to S-matrix unitarity, $R+T=N$, where $R=\mathrm{tr}(r^\dagger r)$ is the reflection coefficient at the left lead. Hence, from Fig. 1, we infer that the average transmission $\langle T \rangle$ is always close to its maximum value, and $\langle T \rangle \gg \langle R \rangle$ in the studied energy range.

Fast processes dominate the transmission when a significant fraction of trajectories connecting left and right leads have dwell times comparable to the traversal time L/v. This is evidently the case for the cosine billiard, since there is a large set of trajectories passing through the billiard inner part after no or only a few bounces.

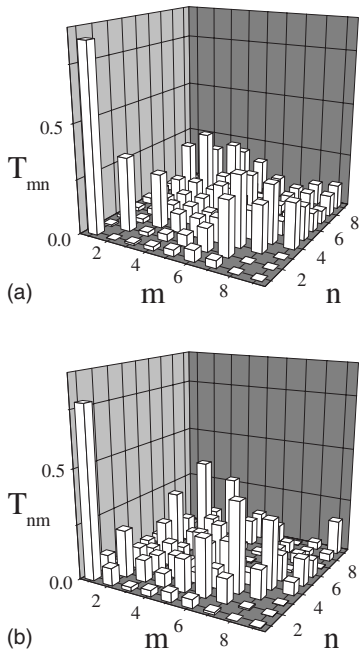

FIG. 2. Partial transmission T_{nm} as a function of m and n, which are the left and right channel numbers, respectively. (a) Classical T_{nm} (independent of energy). (b) Quantum $T_{nm}(E) = |t_{nm}(E)|^2$ for $E = 77.17$ meV.

We can make this statement quantitative by calculating the classical transmission probability $\tilde{T}$ and by comparing to quantum average transmission $\langle T(E) \rangle$. For this purpose, we introduce the partial transmission probability T_{nm}. Classically, T_{nm} is defined as the probability of a trajectory with incident energy $E_\perp \in [(E_\perp)_{m-1}, (E_\perp)_m]$ from the left lead to emerge from the right lead with $E_\perp \in [(E_\perp)_{n-1}, (E_\perp)_n]$. Hence, $\tilde{T} = \Sigma_{m,n} T_{nm}$. For billiards, $\tilde{T}$ depends on the number of channels, but not on the energy. We compute $\tilde{T}$ by a Monte Carlo simulation randomly starting 10^5 trajectories at the left contact. Quantum mechanically, the partial transmission is a function of energy and is defined as $T_{nm}(E) = |t_{nm}(E)|^2$. The agreement between $\tilde{T}$ and $\langle T(E) \rangle$ is remarkably good. For instance, for the $N=9$ plateau, we obtain $\tilde{T} = 8.26$ and $\langle T(E) \rangle = 8.31$. Surprisingly, a reasonable quantitative agreement holds even when we compare classical and quantum partial transmission coefficients taken at a resonance, namely, $|t_{mn}|^2$, as shown in Fig. 2.

These ideas help us to understand the energy averaged transmission $\langle T \rangle$, but they are not fingerprints of mixed dynamics, since nonresonance transmission can also occur in chaotic systems.[41] In its simplest (and best known) formulation, the statistical theory of chaotic scattering does not account for direct processes and predicts $\langle T \rangle \approx \langle R \rangle \approx N/2$ when $N \gg 1$. However, there are various ways to include fast nonresonance processes in the theory,[42,43] which can lead to a $\langle T \rangle$ very dissimilar to $\langle R \rangle$.

Let us now address the transmission fluctuations. To guide our discussion, we use Fig. 3(a), which shows G/G_0 as a function of E for the $N=9$ plateau. The slow transmission fluctuations that occur on the energy scale of $\Gamma_{\mathrm{cor}} \sim 1$ meV are of the order of unity, $\delta T \sim 1$, resembling the universal

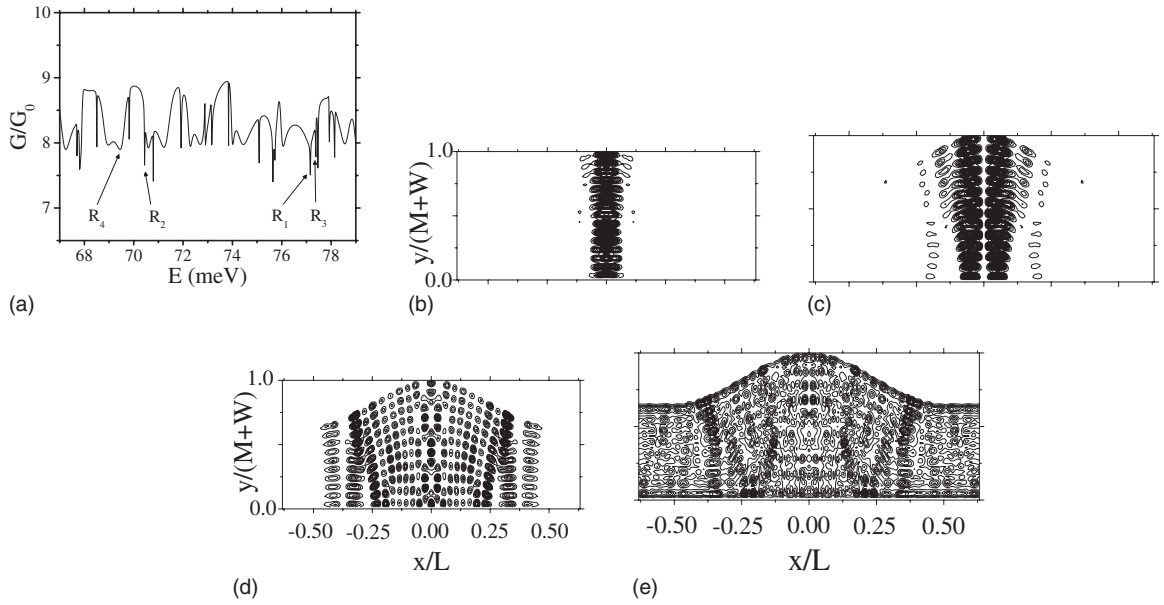

FIG. 3. (a) Conductance in units of $G_0=2e^2/h$ versus energy in meV for the cosine billiard at the plateau $N=9$. Contour plot of the local density of states (in arbitrary units) for selected resonances: (b) R_1 and (c) R_2 are localized states at the stability island; (d) R_3 is an example of a localized state at a cantorus; and (e) R_4 illustrates the generic situation of a delocalized state corresponding to the superposition of many short-lived resonances.

conductance fluctuations typical of resonance scattering in chaotic systems.[2,3] In contrast, we will show that the narrow resonances, whose widths Γ rarely exceed 0.1 meV, correspond to localized states, typical of mixed systems.

The Weyl formula gives a quite accurate estimate for the average resonance spacing Δ, namely, $\Delta=2\pi\hbar^2/m^*\mathcal{A}$, where $\mathcal{A}$ is the area of the cosine billiard. We define $\mathcal{A}$ by closing the billiard at $x=\pm L/2$. The justification is that resonance states of the billiard have close to unit probability to be found inside this boundary (the inner region). This reasoning to assess $\mathcal{A}$ might sound somewhat cavalier, but is semiclassically justified[44] and has been tested by comparing with the average Wigner time delay.[28] For the parameters chosen in this study, the Weyl formula gives $\Delta\approx 0.2$ meV, much smaller than the average spacing between consecutive narrow peaks.

To get further insight, let us examine the LDOS for some selected energies. Many of the narrow resonances are easily identified with localized states at the central stability island. For instance, the resonance R_1 in Fig. 3(a) has an energy that is in good agreement with a Wentzel–Kramers–Brillouin vertical mode passing through $x=0$.[45] The corresponding LDOS is shown as a contour plot in Fig. 3(b). Denser lines indicate a large LDOS, while the empty regions correspond to a smaller LDOS. For R_1, LDOS is 10^3 smaller at the contact region than at x close to the origin. R_2 shows another localized state at the central island [see Fig. 3(c)]. This one is odd under parity transformation $x\rightarrow -x$, possessing a nodal line at $x=0$. Such states spread over a larger region in x than the simple R_1 state. Still their LDOS at the contact region is suppressed by 2 or 3 orders of magnitude with respect to its maximum value.

We also observe that many of the narrow states are clearly not localized at the stability island. A typical example is R_3, whose LDOS is shown in Fig. 3(d). Bäcker *et al.*[29] investigated the nature of such states. By analyzing the Husimi representation of a sequence of narrow states, they showed that a large fraction of them are actually trapped by cantori typical of mixed phase space systems.

Finally, the transmission fluctuations occuring over energy scales larger than Δ are built from the overlap of resonances, corresponding to delocalized states. Figure 3(e) shows the LDOS of R_4, which is a typical example of this situation.

Further evidence supporting this picture is provided by Fig. 4. It shows the transmission as a function of E as we progressively close the billiard with potential barriers placed at the contacts.[46] We consider barriers up to 120 Å wide and

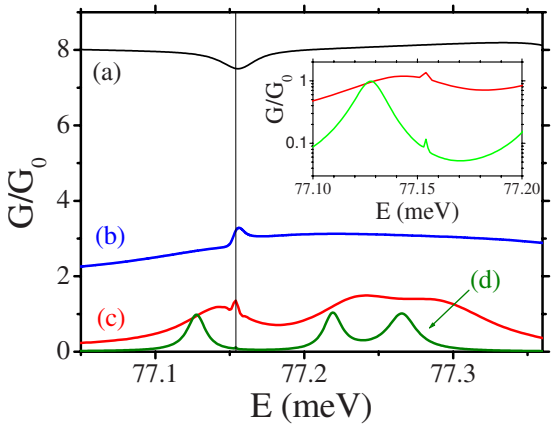

FIG. 4. (Color online) Transmission probability for the cosine billiard over an energy window around the R_1 resonance. The transmission drops from (a) to (d) as barriers placed at the billiard contacts become higher. Inset: Low transmission curves in a logarithmic scale.

250 meV high. Figure 4 shows G/G_0 for a small energy window around the R_1 resonance. For the open billiard [curve (a)], R_1 is a dip in the transmission, which is a typical line shape of a Fano resonance with a large background contribution. Transmission barriers suppress the background, t^{bg}, both from direct processes and overlapping resonances. This is seen in Fig. 4 [in curve (b)] already for a very thin barrier (20 Å wide and 85 meV high): the average transmission drops roughly by a factor 2 and the resonance line shape changes entirely. By further increasing the barrier strength, curves (c) and (d), which are the overlapping resonances corresponding to delocalized states, become isolated. By inspecting a larger energy interval than the one shown in Fig. 4, we find that the average resonance spacing agrees with the Weyl estimate.

These elements lead us to interpret the slow energy dependent fluctuations in the conductance as a coherent superposition of overlapping resonances, with complex poles whose imaginary part is typically larger than Δ. In turn, the narrow resonances, whose widths are much smaller than Δ, correspond to localized states due to the mixed dynamics. The clear separation of energy scales is essential to justify a constant q' and to validate our analysis.

A. Analysis of Fano shapes

By examining partial transmissions $t_{nm}(E)$ at several resonances, we have verified that Eq. (11) accurately describes the Fano transmission line shapes. Our procedure is the following: to restrict the number of free parameters, we first select a resonance ν (like, for instance, R_1) and find the best fit for E_ν and Γ_ν by using several pairs of channels (m,n). To describe the transmission at $|E-E_\nu| \gg \Gamma_\nu$, we approximate $|t^{\mathrm{bg}}_{nm}|^2$ by a linear background, whose slope depends on (m,n). Finally, we fit q' using a χ^2 procedure.

The heuristic alternative to Eq. (11) found in the literature[22] adds a linear background to the standard Fano line shape [Eq. (5)] and uses a real q. For the resonances we examine, we find that fitting Fano line shapes in this way is as effective (in the sense of the reduced χ^2 test) as using a complex q. We attribute the good agreement between both fitting procedures to the large number of free parameters. Figure 5 shows two typical fits.

Can the shapes of both parametrizations differ appreciably? To answer this question, let us explictly consider $q = q_r + iq_i$. Equation (11) corresponds to a sum of a standard Fano resonance, parametrized by q_r and a Breit–Wigner one, whose "weight" is enconded in q_i. When q_r and q_i have comparable magnitudes, the resulting resonance shape can markedly be different from the family of standard Fano shapes. Unfortunately, we did not find such a case in our numerical analysis.

Distinct traces of Fano resonances characterized by a complex q have been experimentally reported for systems with broken time-reversal symmetry.[13] We stress that in the multichannel case, despite the resonances we analyze, real and complex q's give similar quality fits, q is generally a complex parameter, even when time-reversal symmetry is present and dephasing is absent (see the Appendix for a proof).

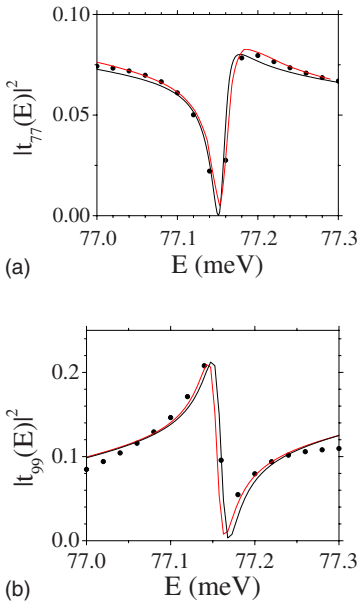

FIG. 5. (Color online) Transmission probability matrix elements for an energy window centered at the resonance R_1. Circles correspond to computed conductance, red lines stand for the best fit using Eq. (11), whereas the black lines correspond to a fit using the standard Fano plus a linear background (see text): (a) $|t_{77}(E)|^2$; (b) $|t_{99}(E)|^2$.

B. Manipulation of Fano shapes

External local probes can be used to selectively manipulate resonances.[23] Suitable choices of the external perturbation allow one to strongly quench selected localized states. Alternatively, with a small change in the billiard shape, one can take full advantage of the numerous resonant transmission interference processes to manipulate the shape of a Fano resonance. The background transmission matrix element t^{bg}_{nm}, given by Eq. (10), accounts for the scattering amplitude of the (neighboring) overlapping resonances to the νth one. It is possible to engineer a small perturbation of the order of $\langle V^2_{\mu\nu}\rangle^{1/2} \sim \Delta$ acting on the QD that dramatically changes t^{bg}_{nm}, without having a significant impact on nonresonant processes.

Figure 6(a) illustrates a situation where both a shift of the localized state R_5 and a dramatic change on the resonance shape R_6 occur. In the absence of a perturbation, the LDOS of R_5 and R_6 are shown in Figs. 6(b) and 6(c), respectively. While R_5 is a localized state around the stable W-shaped periodic orbit, R_6 belongs to the already discussed stability island around $x=0$. The perturbation we consider is a potential step of strength V, indicated by the inset of Fig. 6(a), that destroys the W-shaped orbit.

Let us discuss how the transmission is affected by increasing V. Already at $V=10$ meV, we observe that the R_5 resonance position in the transmission spectrum is significantly shifted. In contrast, the average transmission $\langle T\rangle$ barely changes and the transmission fluctuations show only slight modifications. This suggests that while the perturbation only slightly changes the background resonance interference patterns, the overlap between the stub and the LDOS of the R_5

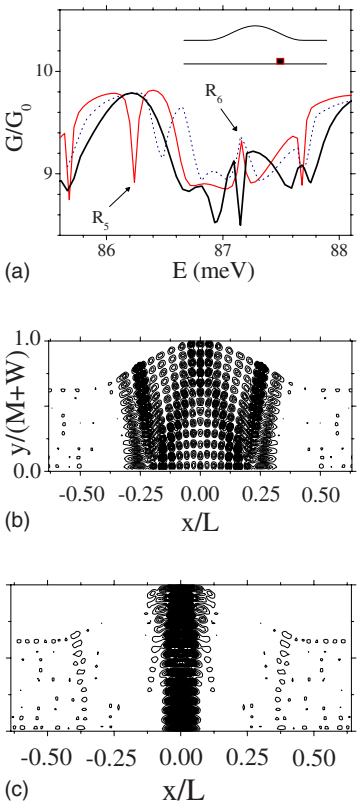

FIG. 6. (Color online) (a) Conductance in units of $2e^2/h$ versus Fermi energy at the $N=10$ plateau for different values of the perturbation V sketched in the inset. The solid red line corresponds to the unperturbed transmission, dotted line to $V=10$ meV, and solid black line to $V=30$ meV. (b) and (c) show the local density of states for the unperturbed resonances R_5 and R_6, respectively.

resonance causes a significant shift on the resonance energy.

By further increasing the perturbation to $V=30$ meV, we observe more pronounced changes in the transmission fluctuations, but still without a noticeable effect in the average transmission. R_5 is further shifted and R_6 is particularly affected: its shape changes from a dip to a Breit–Wigner-like resonance. In this case, the background overlapping resonances control the shape of an isolated resonance not directly affected by the perturbation (negligeble overlap).

VI. CONCLUSIONS

Fano line shapes are ubiquitous in resonance scattering. Whereas they have been reported in mesoscopic transport in QDs at the Coulomb and Kondo regimes, they seem harder to observe in open quantum dots.

We showed that QDs with mixed dynamics show Fano line shapes, whereas such resonances are hardly observed in chaotic QDs. Sharp conductance peaks correspond to localized states that typically coexist with a background of long-lived delocalized states as well as with fast nonresonant processes. Both contribute to the Fano line shapes. This is why, in practice, controlling the shape of transmission resonances can be quite delicate.

Furthermore, we showed that even in the presence of time-reversal symmetry and in the absence of dephasing, the Fano resonance q parameter is generally complex. Unfortunately, a clear assessment of its complex part is not always possible.

Standard magnetoconductance experiments on open quantum dots are unlikely to be suitable for the investigation of Fano resonance physics. In our model, the trajectories contained by the stability island cover only a small area of the billiard inner part. Hence, to observe their contribution to the magnetoconductance, sweeps over very large magnetic fields are required. In addition, it is not yet clear which magnetofingerprints would characterize them.

The transmission energy dependence we studied can be inferred by experiments measuring the conductance as a function of a back gate voltage. For mixed systems, such a possibility was explored in Ref. 47 to locate resonance energies. Temperatures larger than the resonance width Γ obviously wash away the line shapes. For instance, temperatures of the order of 100 mK, standard in low-dilution refrigerators, will have little impact on resonances with $\Gamma \gtrsim 0.05$ meV, but will smear the narrower ones. For realistic model parameters, many of the narrow resonances we observe, particularly those localized in cantori, have widths $\Gamma \lesssim 0.1$ meV.

ACKNOWLEDGMENTS

We thank Piet Brouwer for useful comments regarding the complex q factor. We acknowledge the Brazilian funding agencies CAPES, CNPq, FAPERJ, and FAPESP for supporting our individual grants. This collaboration was also made possible by the Rede Nacional de Nanociências (CNPq/Brazil). C.H.L. thanks the Harvard's Institute of Quantum Science and Engineering for support.

APPENDIX: COMPLEX q PARAMETERS

Here, we show that the Fano parameter q is generally complex for multichannel scattering in time-reversal symmetric systems.

In its most general form, the S matrix for an isolated resonance coupled to N_{tot} open channels reads[42,48]

$$S(E) = U\left(1 - i\frac{\gamma\gamma^T}{E - E_\nu + i\Gamma/2}\right)U^T. \tag{A1}$$

The column vector γ is chosen to be real and satisfies $\gamma^T\gamma = \Gamma$. Background scattering is provided by the unitary matrix U of dimension $N_{\text{tot}} \times N_{\text{tot}}$ through the combination UU^T. In the main text, we considered the case of $N_{\text{tot}}=2N$. The parametrization above is explicitly unitary[35] and symmetric, i.e., $S=S^T$, with the latter property being a necessary consequence of time-reversal symmetry.

A simple calculation leads to the following expression for the Fano parameter describing the line shape of $|t_{nm}(E)|^2$:

$$q = i - \frac{2i}{\Gamma}\frac{U_n^T\gamma\gamma^T U_m}{U_n^T U_m} \tag{A2}$$

[cf. Eq. (12)]. Here, U_n and U_m are the nth and mth rows of U, thought of as column vectors.

For $N_{\text{tot}}=2$, we can write U in terms of the Cayley–Klein parametrization of the SU(2) group to explicitly verify that q is real for any γ and U, as obtained in Ref. 48. For $N_{\text{tot}}>2$, q acquires an imaginary part, whose magnitude depends on γ and U.

It is instructive to compute $\langle q \rangle$, which can be done by taking γ to be uniformly distributed over the sphere of radius $\sqrt{\Gamma}$. By using[49]

$$\langle \gamma \gamma^T \rangle = \frac{\Gamma}{N_{\text{tot}}} \mathbb{1}, \tag{A3}$$

we arrive at

$$\langle q \rangle = i \frac{N_{\text{tot}} - 2}{N_{\text{tot}}}. \tag{A4}$$

This proves that q is, indeed (in general), complex for $N_{\text{tot}}>2$. The $N_{\text{tot}}=2$ case gives $\langle q \rangle = 0$, consistent with $\text{Im}(q)=0$, as it should.[48]

[1] Y. Imry, *Introduction to Mesoscopic Physics* (Oxford University Press, New York, 1997).
[2] I. L. Aleiner, P. W. Brouwer, and L. I. Glazman, Phys. Rep. **358**, 309 (2002).
[3] Y. Alhassid, Rev. Mod. Phys. **72**, 895 (2000).
[4] H. U. Baranger, R. A. Jalabert, and A. D. Stone, Chaos **3**, 665 (1993); R. O. Vallejos and C. H. Lewenkopf, J. Phys. A **34**, 2713 (2001).
[5] U. Fano, Phys. Rev. **124**, 1866 (1961).
[6] R. K. Adair, C. K. Bockelman, and R. E. Peterson, Phys. Rev. **76**, 308 (1949).
[7] U. Fano and A. R. P. Rau, *Atomic Collisions and Spectra* (Academic, Orlando, 1986).
[8] F. Cerdeira, T. A. Fjeldly, and M. Cardona, Phys. Rev. B **8**, 4734 (1973).
[9] J. Faist, F. Capasso, C. Sirtori, K. W. West, and L. N. Pfeiffer, Nature (London) **390**, 589 (1997); H. Schmidt, K. L. Campman, A. C. Gossard, and A. Imamoglu, Appl. Phys. Lett. **70**, 3455 (1997).
[10] V. Madhavan, W. Chen, T. Jamneala, M. Crommie, and S. Wingreen, Science **280**, 567 (1998).
[11] S. Rotter, F. Libisch, J. Burgdörfer, U. Kuhl, and H.-J. Stöckmann, Phys. Rev. E **69**, 046208 (2004).
[12] J. Göres, D. Goldhaber-Gordon, S. Heemeyer, M. A. Kastner, H. Shtrikman, D. Mahalu, and U. Meirav, Phys. Rev. B **62**, 2188 (2000).
[13] K. Kobayashi, H. Aikawa, S. Katsumoto, and Y. Iye, Phys. Rev. Lett. **88**, 256806 (2002); Phys. Rev. B **68**, 235304 (2003).
[14] K. Kobayashi, H. Aikawa, A. Sano, S. Katsumoto, and Y. Iye, Phys. Rev. B **70**, 035319 (2004); M. Sato, H. Aikawa, K. Kobayashi, S. Katsumoto, and Y. Iye, Phys. Rev. Lett. **95**, 066801 (2005).
[15] A. C. Johnson, C. M. Marcus, M. P. Hanson, and A. C. Gossard, Phys. Rev. Lett. **93**, 106803 (2004).
[16] A. Fuhrer, P. Brusheim, T. Ihn, M. Sigrist, K. Ensslin, W. Wegscheider, and M. Bichler, Phys. Rev. B **73**, 205326 (2006).
[17] J. L. D'Amato, H. M. Pastawski, and J. F. Weisz, Phys. Rev. B **39**, 3554 (1989).
[18] E. Tekman and P. F. Bagwell, Phys. Rev. B **48**, 2553 (1993).
[19] J. U. Nöckel, and A. D. Stone, Phys. Rev. B **50**, 17415 (1994).
[20] W. Porod, Z. Shao, and C. Lent, Phys. Rev. B **48**, 8495 (1993).
[21] J. P. Bird, *Electron Transport in Quantum Dots* (Kluwer Academic, Dordrect, 2003), p. 209.
[22] B. Weingartner, S. Rotter, and J. Burgdörfer, Phys. Rev. B **72**, 115342 (2005).
[23] M. Mendoza and P. A. Schulz, Phys. Rev. B **71**, 245303 (2005).
[24] L. G. Mourokh, V. I. Puller, A. Yu. Smirnov, and J. P. Bird, Appl. Phys. Lett. **87**, 192501 (2005).
[25] Y. Takagaki and K. H. Ploog, Phys. Rev. B **64**, 245336 (2001).
[26] J. P. Bird, R. Akis, D. K. Ferry, D. Vasileska, J. Cooper, Y. Aoyagi, and T. Sugano, Phys. Rev. Lett. **82**, 4691 (1999); R. Crook, C. G. Smith, A. C. Graham, I. Farrer, H. E. Beere, and D. A. Ritchie, *ibid.* **91**, 246803 (2003); B. Hackens, S. Faniel, C. Gustin, X. Wallart, S. Bollaert, A. Cappy, and V. Bayot, *ibid.* **94**, 146802 (2005); A. G. Huibers, S. R. Patel, C. M. Marcus, P. W. Brouwer, C. I. Duruoz, and J. S. Harris, *ibid.* **81**, 1917 (1998); I. V. Zozoulenko, R. Schuster, K. F. Berggren, and K. Ensslin, Phys. Rev. B **55**, R10209 (1997).
[27] G. A. Luna-Acosta, K. Na, L. E. Reichl, and A. Krokhin, Phys. Rev. E **53**, 3271 (1996); G. A. Luna-Acosta, A. A. Krohkin, M. A. Rodríguez, and P. H. Hernández-Tejeda, Phys. Rev. B **54**, 11410 (1996).
[28] B. Huckestein, R. Ketzmerick, and C. H. Lewenkopf, Phys. Rev. Lett. **84**, 5504 (2000).
[29] A. Bäcker, A. Manze, B. Huckestein, and R. Ketzmerick, Phys. Rev. E **66**, 016211 (2002).
[30] P. A. Mello and N. Kumar, *Quantum Transport in Mesoscopic Physics* (Oxford University Press, Oxford, 2003).
[31] D. S. Fisher and P. A. Lee, Phys. Rev. B **23**, 6851 (1981).
[32] S. Datta, *Electronic Transport in Mesoscopic Systems* (Cambridge University Press, Cambridge, 1996).
[33] F. Sols, M. Macucci, U. Ravaioli, and K. Hess, J. Appl. Phys. **66**, 3892 (1989).
[34] H. U. Baranger, D. P. DiVincenzo, R. A. Jalabert, and A. D. Stone, Phys. Rev. B **44**, 10637 (1991).
[35] J. R. Taylor, *Scattering Theory: The Quantum Theory of Nonrelativistic Collisions* (Wiley, New York, 1972).
[36] V. V. Sokolov and V. G. Zelevinsky, Ann. Phys. (N.Y.) **216**, 323 (1992).
[37] T. Nakanishi, K. Terakura, and T. Ando, Phys. Rev. B **69**, 115307 (2004).
[38] A. I. Magunov, I. Rotter, and S. I. Strakhova, Phys. Rev. B **68**, 245305 (2003).
[39] S. Klaiman, N. Moiseyev, and H. R. Sadeghpour, Phys. Rev. B **75**, 113305 (2007).
[40] Y. Berlatzky and S. Klaiman, arXiv:0709.2548 (unpublished).

[41] C. H. Lewenkopf and H. A. Weidenmüller, Ann. Phys. (N.Y.) **212**, 53 (1991).
[42] C. A. Engelbrecht and H. A. Weidenmüller, Phys. Rev. C **8**, 859 (1973); H. Nishioka and H. A. Weidenmüller, Phys. Lett. **157B**, 101 (1985).
[43] P. A. Mello, P. Pereyra, and T. H. Seligman, Ann. Phys. (N.Y.) **161**, 254 (1985).
[44] R. O. Vallejos, A. M. Ozorio de Almeida, and C. H. Lewenkopf, J. Phys. A **31**, 4885 (1998).
[45] R. O. Vallejos, C. H. Lewenkopf, M. Mendoza, and P. A. Schulz (unpublished).
[46] This construction serves only to provide insight into the transmission resonances. The theory of electronic transport in quantum dots through states with a long lifetime has to account for charging effects.
[47] A. P. S. de Moura, Y.-C. Lai, R. Akis, J. P. Bird, and D. K. Ferry, Phys. Rev. Lett. **88**, 236804 (2002).
[48] A. A. Clerk, X. Waintal, and P. W. Brouwer, Phys. Rev. Lett. **86**, 4636 (2001).
[49] M. L. Mehta, *Random Matrices*, 3rd ed. (Academic, Amsterdam, 2004).